

### **Supplementary Figure 1: DNMT1, but not DNMT3a and 3b, is flow sensitive**

**(A)** Representative immunohistochemical staining of DNMT3a and DNMT3b protein (red) in carotid artery (LCA or RCA) sections at 2 days post-ligation in C57BL/6 mice. Nuclei are stained with DAPI in blue and the elastin laminae autofluoresce green. L indicates the lumen of the blood vessel. (scale bar = 100  $\mu$ m) **(B)** Representative immunohistochemical staining of DNMT1, DNMT3a, and DNMT3b protein (red) in the naturally flow-disturbed lesser curvature (LC) and unidirectional flow greater curvature (GC) and thoracic aorta (TA) in C57BL/6 mice. Nuclei are stained with DAPI in blue and the elastin laminae autofluoresce green. (scale bar = 50  $\mu$ m)

### **Supplementary Figure 2: 5-Aza-2'-deoxycytidine (5Aza) decreases DNMT1 protein expression, activity, and global DNA methylation in HUVECs**

**(A,B)** Western blot of DNMT1 and DNMT3b protein expression in static HUVEC cells treated with 0, 0.5, 1, 5, and 20  $\mu$ M 5Aza for 5 days (A). HeLa extract is used in both blots as a positive control, and blots are normalized to  $\beta$ -actin. DNMT enzymatic activity in HUVECs treated with 0, 0.5, 1, 5, and 20  $\mu$ M 5Aza for 5 days was determined. Data are shown as mean  $\pm$  s.e.m; \*  $p < 0.05$ , \*\*  $p < 0.01$ ,  $n=3$  each. (B). **(C)** Western blot was done to determine DNMT1 and DNMT3b protein expression in lysates of HUVECs subjected to 24 hours of LS or OS with either a 5 day pre-treatment with 5  $\mu$ M 5Aza or vehicle control, and was normalized to  $\beta$ -actin. **(D)** DNMT enzymatic activity was determined using lysates of HUVECs subjected to 24 hours of LS or OS with either a 5 day pre-treatment with 5  $\mu$ M 5Aza or vehicle control. Data are shown as mean  $\pm$  s.e.m; \*  $p < 0.05$ , \*\*  $p < 0.01$ ,  $n=6$  each. **(E)** The gel shows the MspI/HpaII methylation restriction enzyme assay result showing that global methylation of genomic DNA (indicated by the arrow) was prevented in static HUVECs treated with 5 $\mu$ M 5Aza for 5 days.

### **Supplementary Figure 3: 5Aza treatment inhibits immune cell infiltration and DNA methylation in mice.**

**(A)** Representative immunohistochemical staining of CD45 (red) in the LCA of the acute, d-flow induced atherosclerosis model, demonstrating a dose-dependent

decrease in immune cell infiltration after 4 weeks of 5Aza treatment from 0.1-0.4 mg/kg/day doses compared to the vehicle control (scale bar = 100  $\mu$ m). **(B-C)** Representative images show immunostaining of 5-methylcytosine **(B)** and DNMT1 **(C)** in red in LCA frozen sections from the partially-ligated ApoE<sup>-/-</sup> mice as described in Figure 3, demonstrating a dose-dependent decrease in global DNA methylation and DNMT1 expression by 5Aza treatment (scale bars = 50  $\mu$ m). Nuclei are stained with DAPI in blue and the elastin laminae autofluoresce green.

**Supplementary Figure 4: 5Aza has no major effects on serum lipid profiles and body weight.**

**(A,C)** Total blood serum cholesterol, triglycerides (TG), high density lipoprotein (HDL), and low density lipoprotein (LDL) in the acute, d-flow induced atherosclerosis model (A) and the chronic, diet-induced atherosclerosis model. Blood was collected from mice immediately before sacrifice. **(B,D)** Mouse body weights were measured weekly over the course of the 5Aza treatment in the acute, d-flow induced atherosclerosis model and in the chronic, diet-induced atherosclerosis model.

**Supplementary Figure 5: 5Aza treatment reduces global methylation in mouse blood cells.**

**(A,B)** High resolution melt curve analysis shows decreased methylation in the normally highly methylated LINE1 (A) and B1 (B) repeat elements of the genome. The analysis was done on blood genomic DNA collected by submandibular bleed just before beginning the 5Aza treatment and one week after the start of the daily 0.2 mg/kg/day 5Aza injections. (n=20; mean  $\pm$  s.e.m; \* p<0.05)

**Supplementary Figure 6: Emergent methylation pattern analysis and genome-wide methylation and gene expression patterns in partially-ligated mouse carotids.**

**(A)** Analysis of gDNA methylation patterns existing in the RRBS datasets by ranking promoter methylation per gene for each RRBS sample (LCA=L, RCA=R, Aza-LCA = aL, and Aza-RCA= aR) revealed a pronounced emergent methylation pattern wherein gene

promoters in the LCA are most methylated as compared to the RCA, Aza-LCA, and Aza-RCA (in decreasing order). **(B-C)** Heatmap correlation scatterplots of the methylomes of the LCA compared to the Aza-LCA and the RCA compared to the Aza-RCA. **(D,E)** Gene expression was compared between the LCA vs. Aza-LCA and RCA vs. Aza-RCA obtained from endothelial RNA as described in Figure 4.

**Supplementary Figure 7: Global comparison of the RRBS data and the transcriptome data demonstrates that our datasets follow expected trends.**

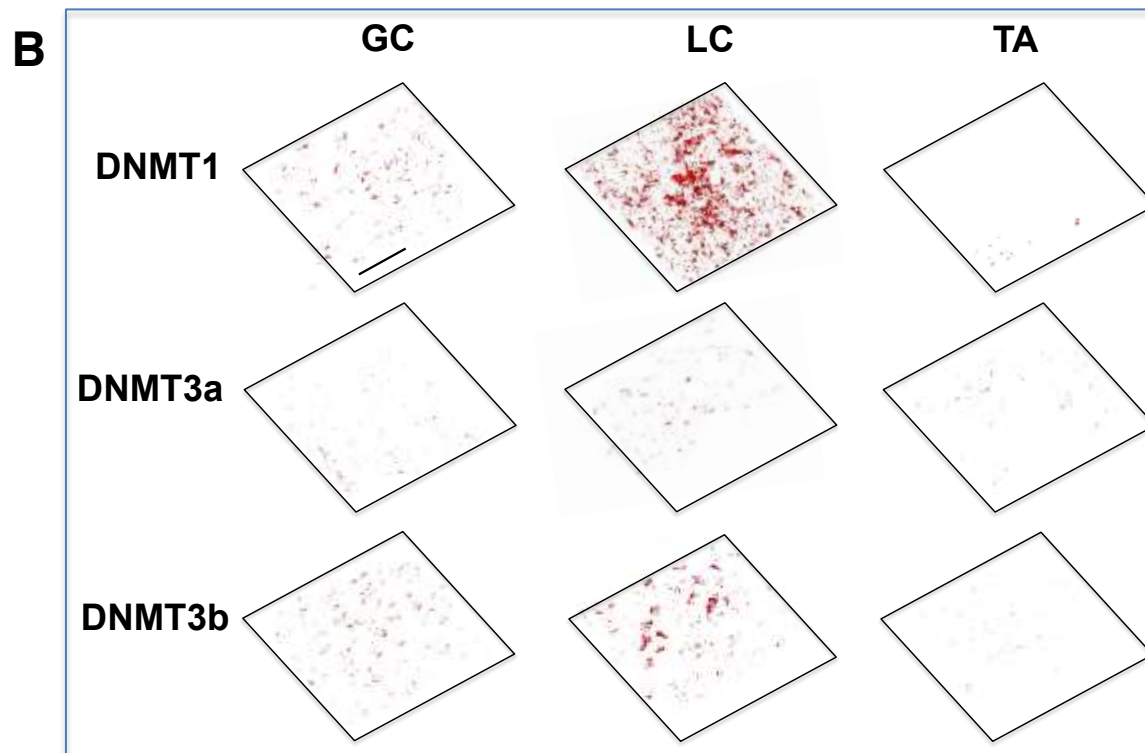
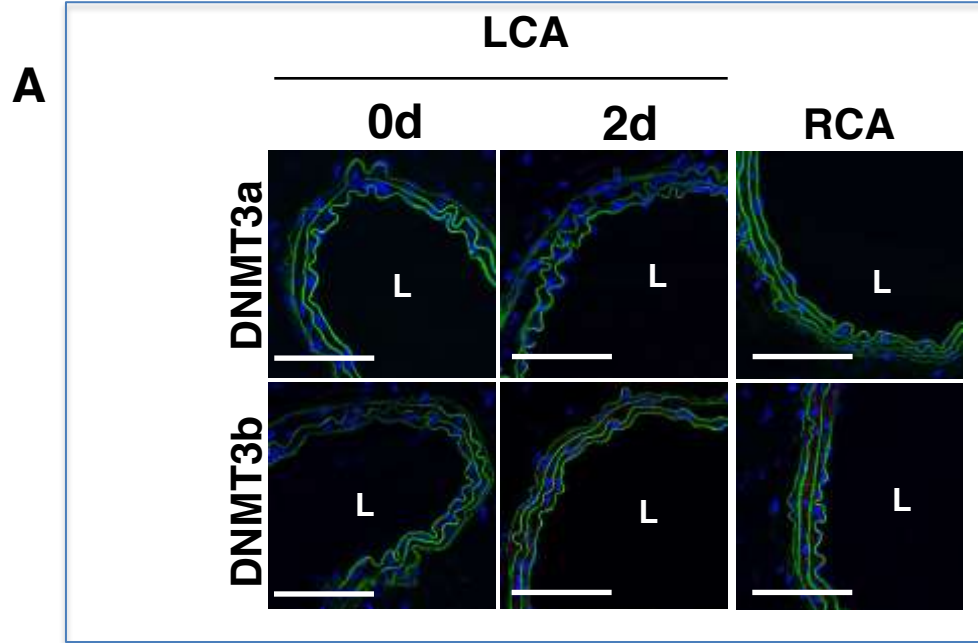
**(A)** Figure A shows a comparison of DNA methylation to gene expression for different regions of the genome: the transcription start site (TSS; the promoter is defined as within  $\pm 1$ kb of a gene TSS), gene body (GB), and transcription termination site (TTS; defined as within  $\pm 1$ kb of a gene TTS). The data for TSS shows the expected inverse correlation between promoter methylation and gene expression. **(B)** Global percent methylation for each of the RRBS datasets was calculated by averaging the methylation ratios across each CG site in the genome or only within promoter regions.

**Supplementary Figure 8: siRNA dose curve optimization for gene knockdown efficiency.**

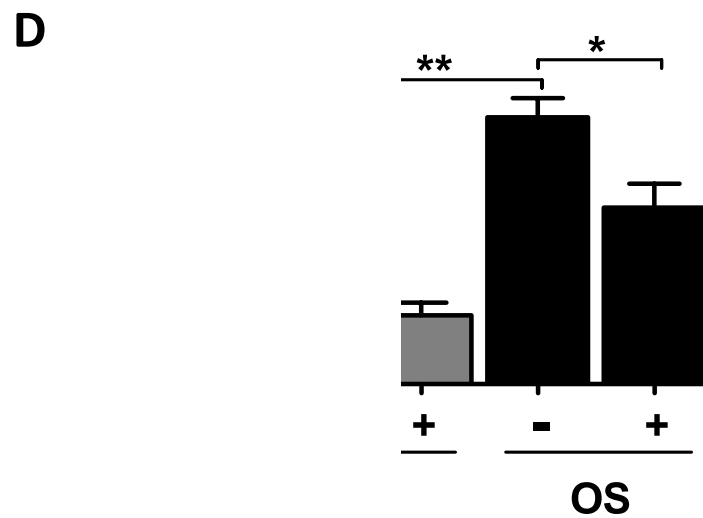
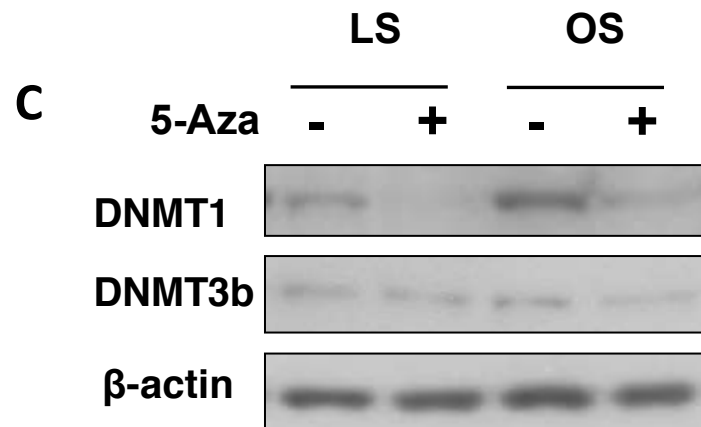
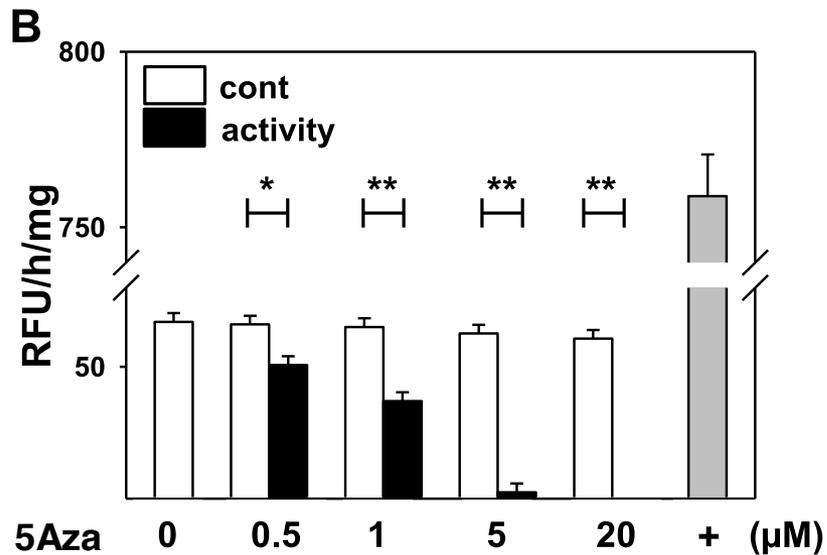
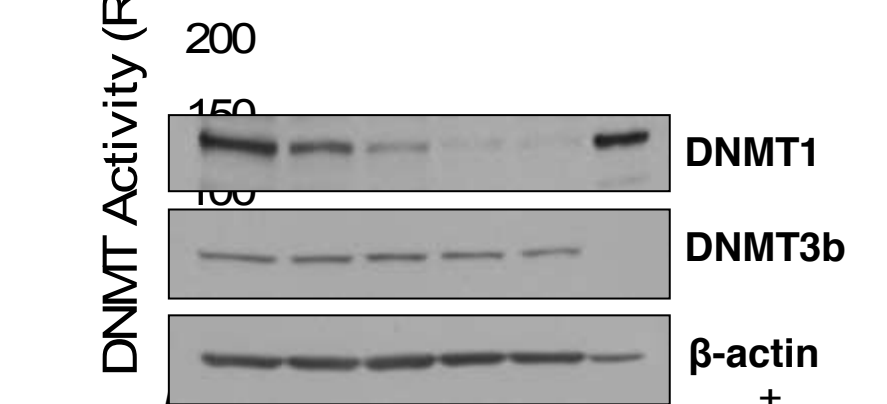
**(A-B)** Static HUVECs were treated with siRNA for HoxA5 **(A)** and Klf3 **(B)** at 50, 100, 150, or 200nM concentrations for 48 hours. The gene expression data is shown using 18s as an internal control, and normalized to the equivalent non-targeting control (NTC) siRNA treatment (n=2; qPCR performed in triplicate). The minimum effective concentration of 100nM was used for studies in Figure 9C and D.

**Supplementary Table 1: The number of CG sites in the Mm9 Genome Assembly and in each RRBS dataset, and the number of CG sites specifically in gene promoter regions (transcription start site  $\pm 1$ kb) in each.**

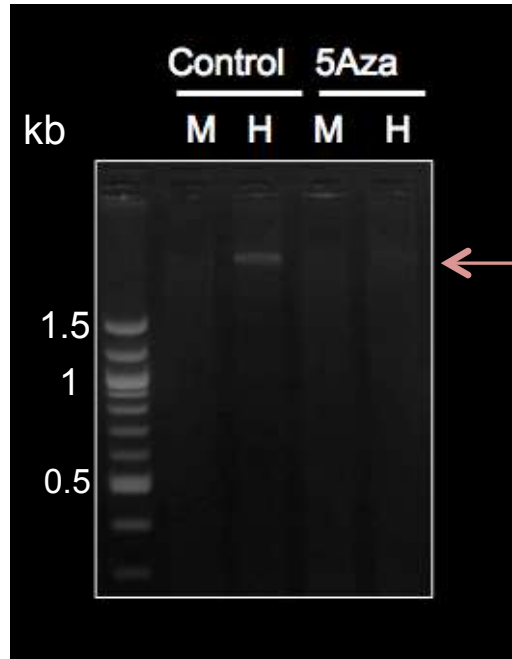
**Supplementary Table 2. Primers used for qPCR or bisulfite sequencing (BS-Seq)**

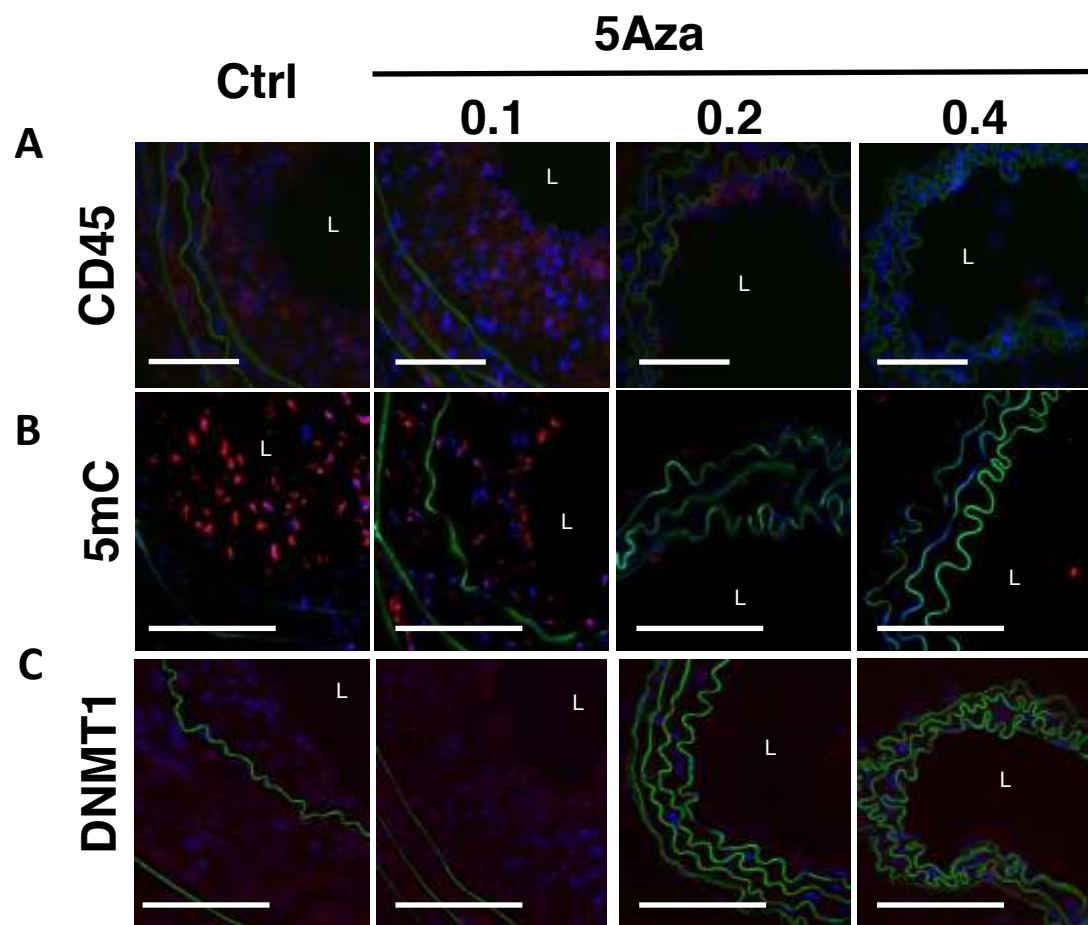


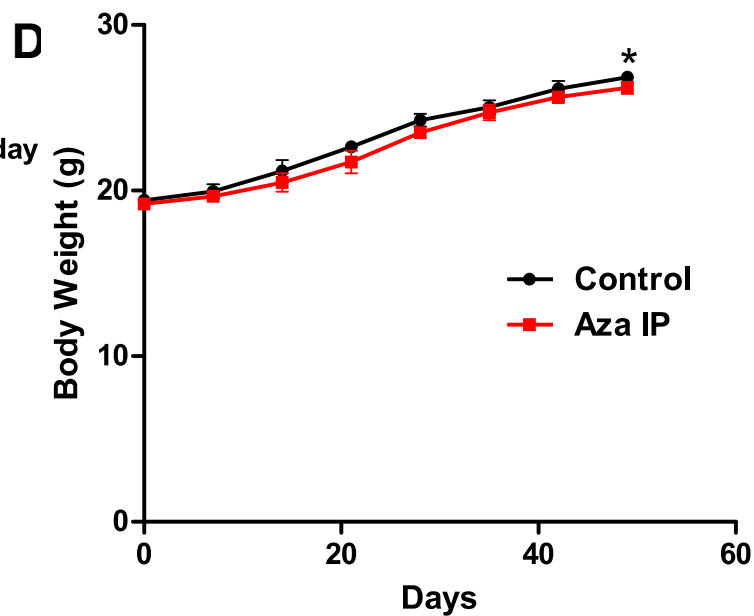
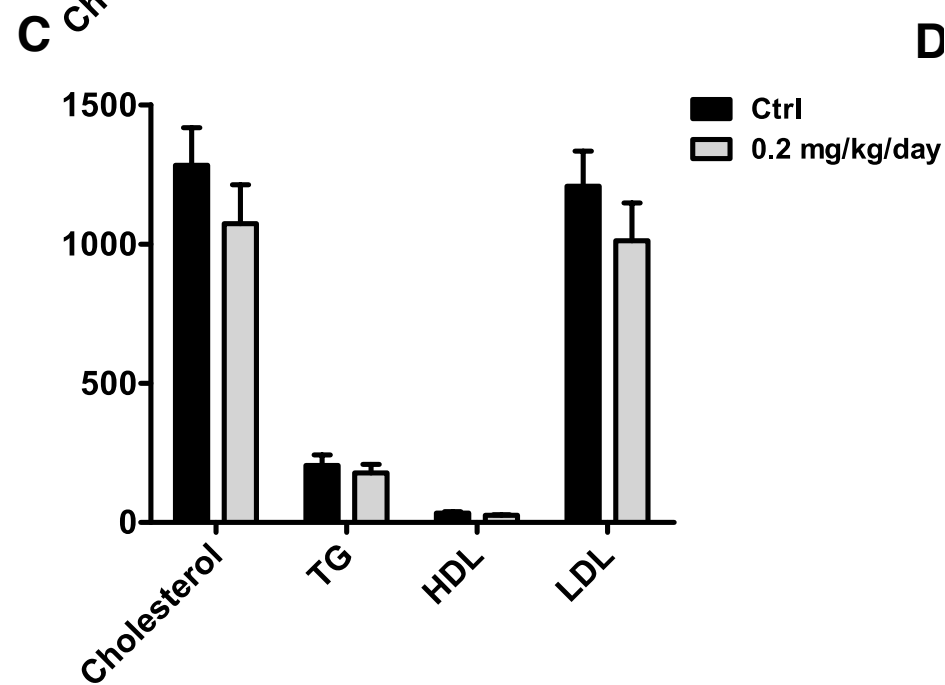
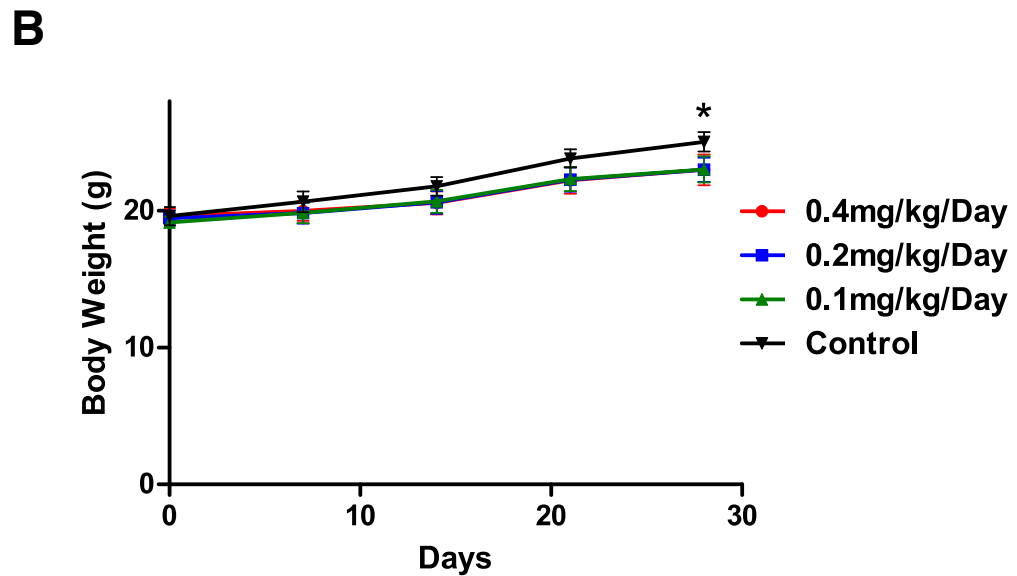
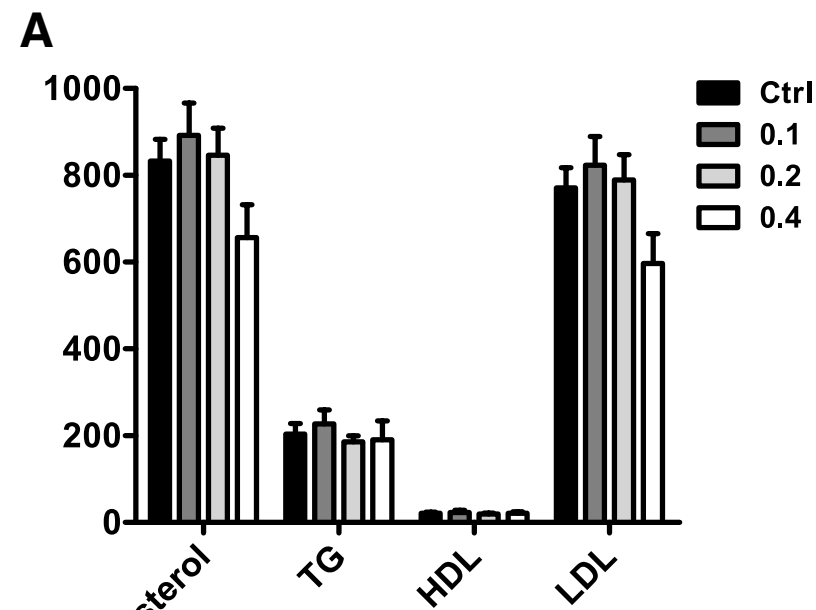
Suppl. Figure 2

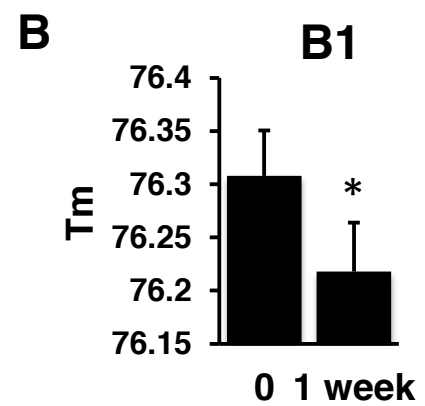
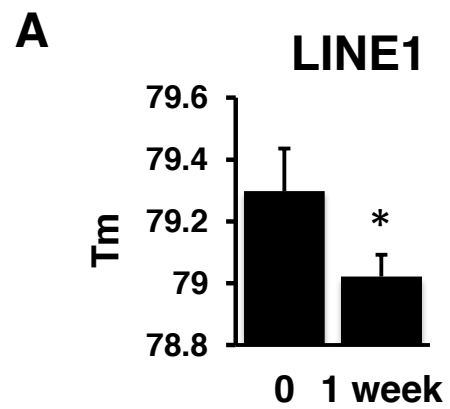


**E**

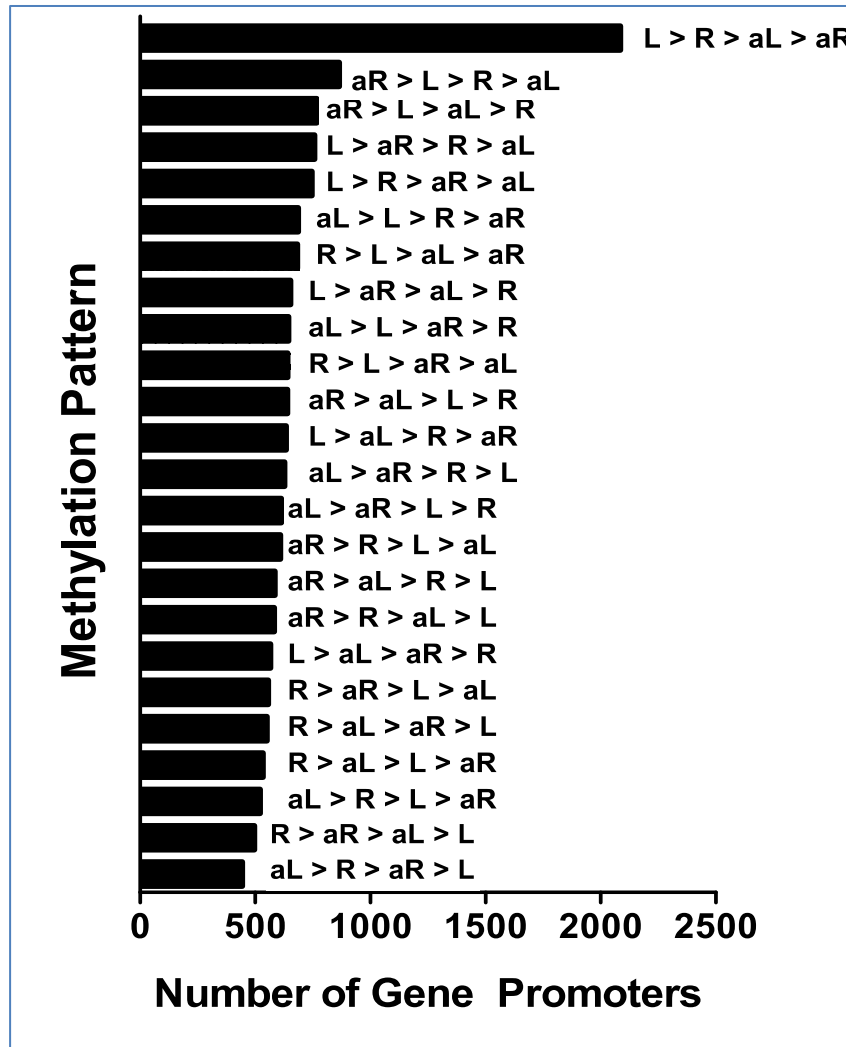






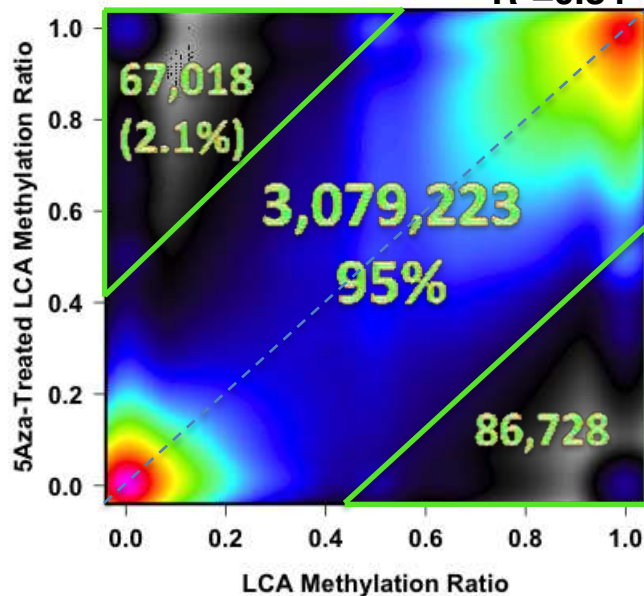


A



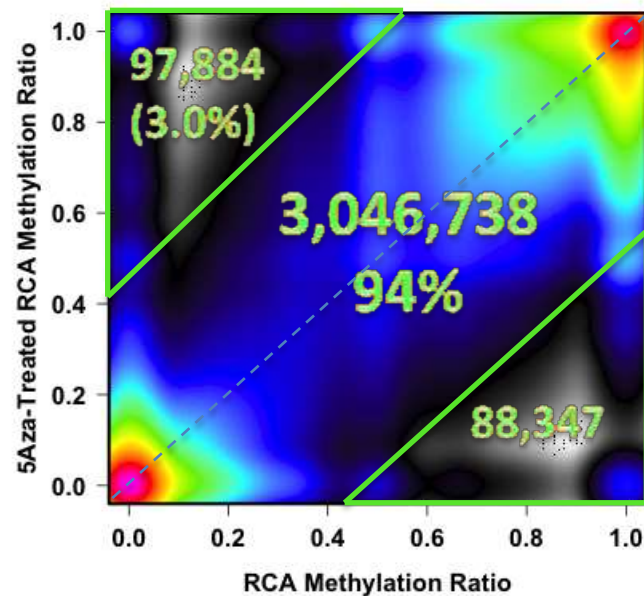
### B. LCA v Aza-LCA

$R^2=0.84$



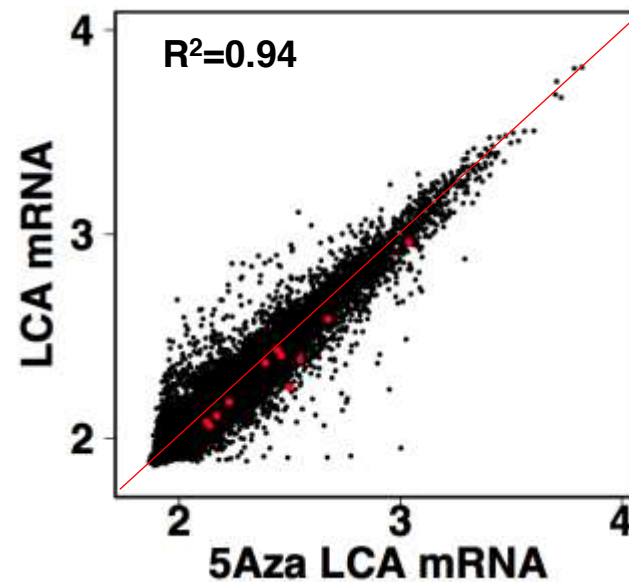
### C. RCA v Aza-RCA

$R^2=0.81$



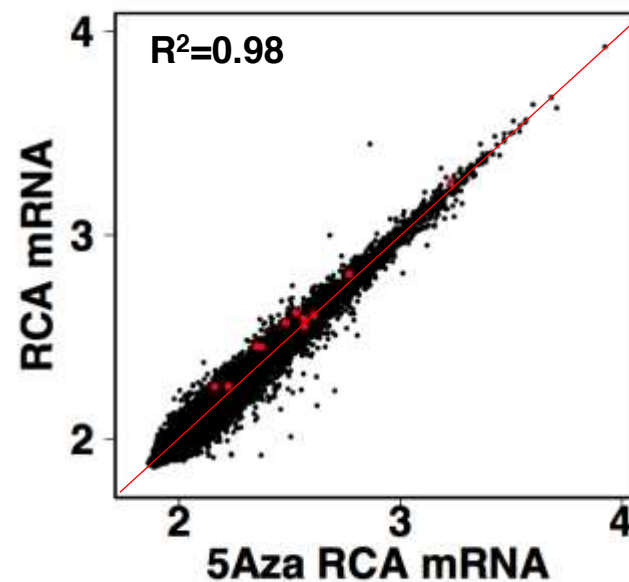
### D. LCA v Aza-LCA

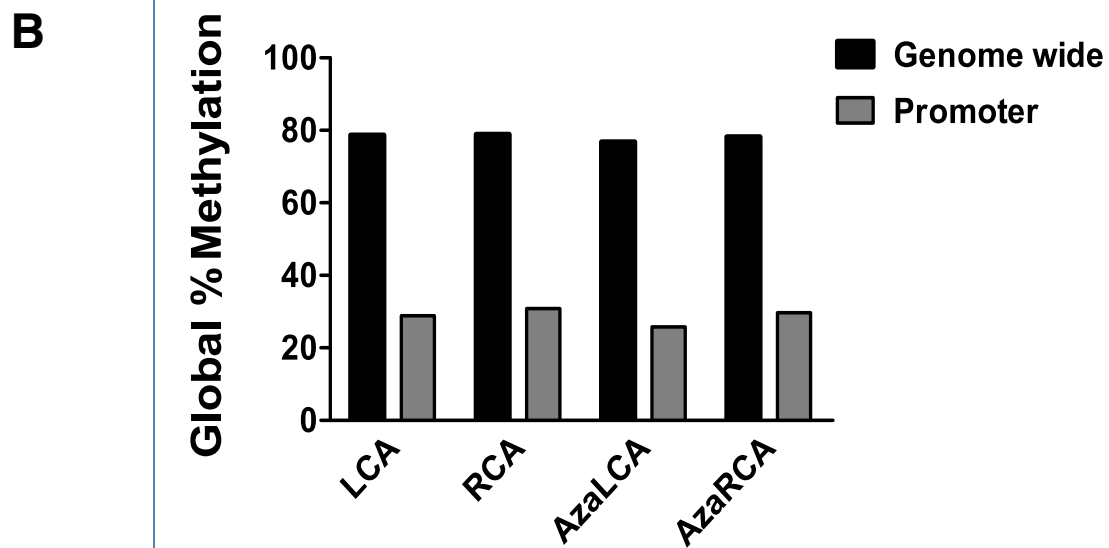
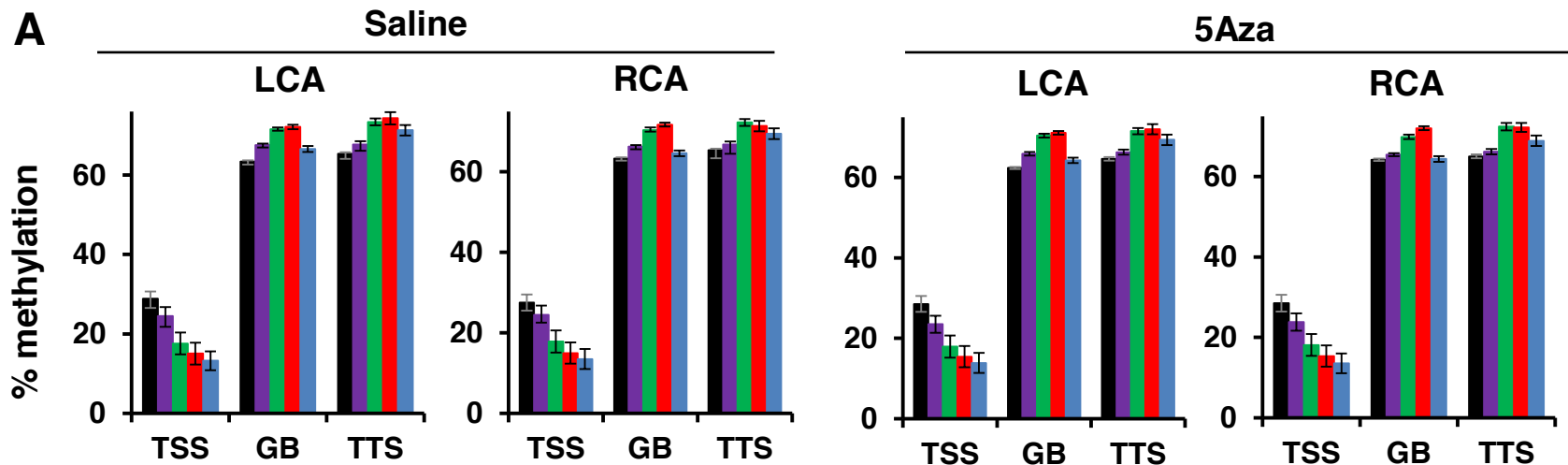
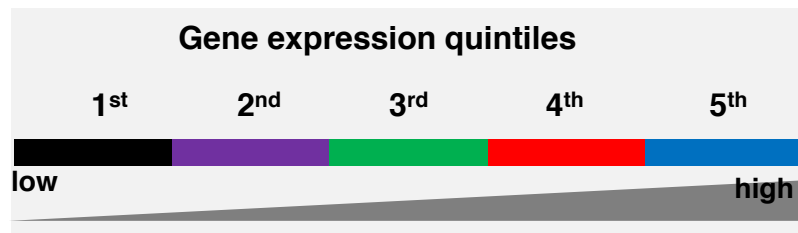
$R^2=0.94$

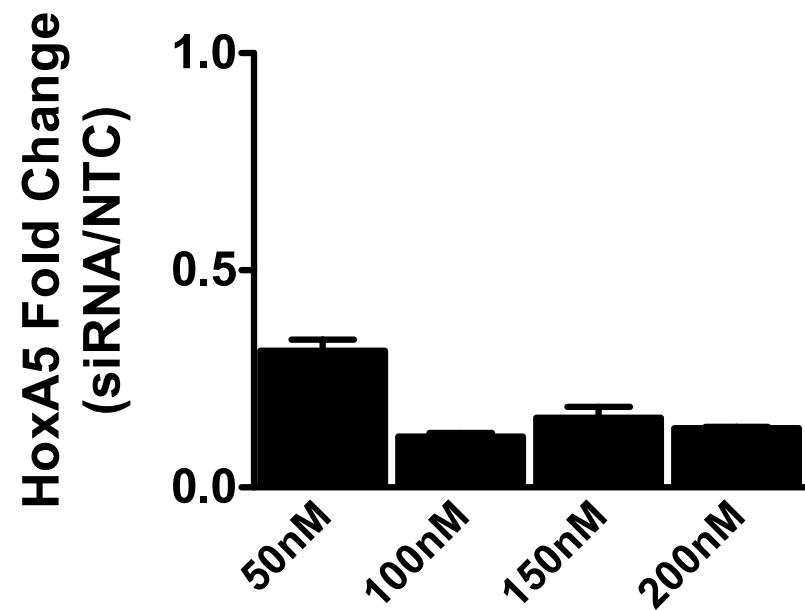
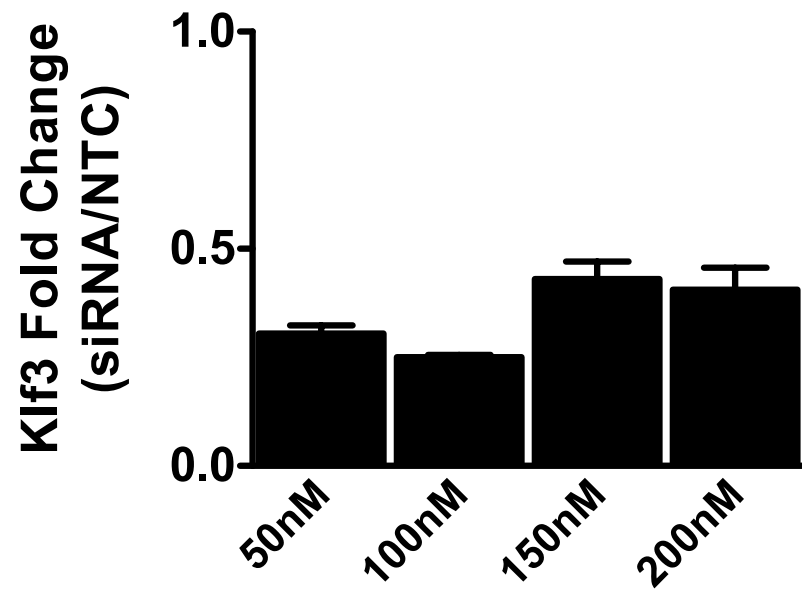


### E. RCA v Aza-RCA

$R^2=0.98$





**A****B**

	<b>Dataset</b>	<b>Total CGs</b>	<b>CGs in Promoters</b>
	Mm9 Genome Assembly	21,342,492	2,130,470
<b>RRBS Datasets</b>	LCA	4,923,836	1,124,726
	RCA	4,584,088	1,068,670
	Aza-LCA	5,308,692	1,156,804
	Aza-RCA	5,054,246	1,153,786
	Average	4,967,716	1,125,997

	<b>Forward</b>	<b>Reverse</b>
<b>DNMT1 ( mouse)</b>	AAGGGGGGCCCTGACCGCTTC	CCGAAATGCCTGGGCTGCCG
<b>DNMT1 (human)</b>	TGCCAGCTGAGCGTGGTGGT	GCATGCGGGCAGCCACCAAT
<b>DNMT3a (mouse)</b>	GAGGGAACTGAGACCCAC	CTGGAAGGTGAGTCTTGGCA
<b>DNMT3b (mouse)</b>	CGCACAACCAATGACTCTGCTG	GGTGACTTCAGAAGCCATCCGT
<b>HoxA5 (mouse)</b>	CGCAAGCTGCACATTAGTCACG	GAGAGGCAAAGGGCATGAGCTA
<b>HoxA5 (human)</b>	GCGCAAGCTGCACATAAG	CGGTTGAAGTGGAACCTCTT
<b>Klf3 (mouse)</b>	CCTCTCATGGTTTCCTTGTCGG	CCTCTGTGGTTCAATTCCAGGC
<b>Klf3 (human)</b>	CTCATGGTCTCCTTATCGGAGG	TGTCCTCTGTGGTTCGATCCCA
<b>HoxA5 BS-Seq (mouse)</b>	GAATTGAGGTTATAGTTTATTATGGTAAAA	AATTATTATAAATAATTCTAAATCACCACC

Suppl. Table 2